Thermalization of non-Abelian gauge theories at next-to-leading order

Yu Fu,[1] Jacopo Ghiglieri,[2] Shahin Iqbal,[1,*,†] and Aleksi Kurkela[3]

[1]*Key Laboratory of Quark and Lepton Physics (MOE) and Institute of Particle Physics, Central China Normal University, Wuhan 430079, China*

[2]*SUBATECH, Université de Nantes, IMT Atlantique, IN2P3/CNRS, 4 rue Alfred Kastler, La Chantrerie Boîte Postale 20722, 44307 Nantes, France*

[3]*Faculty of Science and Technology, University of Stavanger, 4036 Stavanger, Norway*

(Received 19 October 2021; accepted 1 March 2022; published 29 March 2022)

We provide the first next-to-leading-order (NLO) weak-coupling description of the thermalization process of far-from-equilibrium systems in non-Abelian gauge theory. We study isotropic systems starting from either over- or underoccupied initial conditions and follow their time evolution toward thermal equilibrium by numerically solving the QCD effective kinetic theory at NLO accuracy. We find that the NLO corrections remain well under control for a wide range of couplings and that the overall effect of NLO corrections is to reduce the time needed to reach thermal equilibrium in the systems considered.

DOI: 10.1103/PhysRevD.105.054031

I. INTRODUCTION

How non-Abelian gauge fields pushed far from equilibrium approach the thermal state is a central question in several branches of physics. In cosmology, far-from-equilibrium configurations of non-Abelian fields may be produced during (p)reheating [1–4], caused by first-order transitions [1,5,6], and are a necessary ingredient for baryogenesis [7,8]. In all of these cases, an understanding of thermalization rates is required for quantitative descriptions of these phenomena [9,10]. In the early stages of ultrarelativistic heavy-ion collisions, a far-from-equilibrium system of gluons and quarks is created. If and how this system reaches local thermal equilibrium plays a crucial part in the phenomenological modeling of the collisions. The recent discussion about the physical origin of collectivity in smaller collision systems created in p-Pb and light-ion collisions [11] further emphasizes the importance of a quantitative understanding of thermalization in far-from-equilibrium systems. Furthermore, connections between systems created in atomic physics experiments and gauge field models are being actively studied (see, e.g., Refs. [12–14]).

While first-principles nonperturbative lattice simulation of far-from-equilibrium quantum systems remains elusive, the past years have witnessed progress in methods relying on different approximations—see Refs. [15,16] for recent reviews. On one hand, holographic methods have been successful in the description of $\mathcal{N} = 4$ super–Yang-Mills theory in the limit of large number of colors N_c and large t'Hooft coupling $\lambda = g^2 N_c$. These studies have advanced to a mature level, even including subleading corrections in the t'Hooft coupling [17,18]. On the other hand, weak-coupling methods are available for generic theories and have also been widely studied. The first works studying thermalization of pure Yang-Mills theory from simple initial conditions [19] have been extended to QCD [20–23], and calculations based on this physical picture have been extended to describe systems of enough complexity to be used in realistic phenomenological modeling of heavy-ion collisions [24,25] and even in light-ion collisions [26]. This picture has also been applied to parametric estimates of thermalization times during reheating [27–29]. These studies have, however, been at best limited to leading order (LO) in the coupling constant, and it is important to improve the accuracy—and, in particular, to test the validity and robustness of the weak-coupling expansion—by finding the first subleading corrections to the weak-coupling results. In this paper, we provide the first numerical description of thermalization from simple, isotropic initial conditions at next-to-leading order (NLO).

A direct diagrammatic description of thermalization is prohibitively difficult due to a need to resum diagrams of all loop orders even to obtain a LO result in λ [30]. At this order, this resummation can be elegantly performed by considering an effective kinetic theory (EKT) that contains all the necessary processes required for a leading-order description of the evolution of the particle distribution functions f [31]. In gauge theories, the derivation of the collision kernels

*shahin@ccnu.edu.cn

†On leave from the National Centre for Physics, Quaid-i-Azam University, Islamabad 44000, Pakistan.

required for the EKT is further nonperturbative [32]. This arises from the Bose enhancement of "soft" infrared modes at the plasma screening scale $m^2 \sim \lambda \int d^3p f/p$, whose interactions with the typical "hard" particles (with $p \sim \langle p \rangle$) are nonperturbative. This, combined with the well-known soft and collinear divergences of the unresummed QCD cross sections, necessitates a resummation that incorporates the physics of in-medium screening [33] and Landau-Pomeranchuk-Migdal (LPM) [34–36] suppression in the QCD effective kinetic theory [32].

The physical picture of EKT can be extended to next-to-leading-order accuracy. The NLO corrections arise from the interactions among the soft modes. The resulting terms are suppressed only by $m/\langle p \rangle \gtrsim \lambda^{1/2}$, in contrast to λ in vacuum field theory. While various NLO corrections to equilibrium and near-equilibrium quantities have been computed [37–42], the framework has not until now been pushed to study thermalization of far-from-equilibrium systems.

In this paper, we extend the NLO formulation of EKT to isotropic far-from-equilibrium systems and apply it to numerically describe thermalization of two specific systems initialized with either under- or overoccupied initial conditions studied in LO in Ref. [19]. In the idealized limit of weak-coupling, thermalization of underoccupied systems (including those created in heavy-ion collisions) proceeds through the process of *bottom-up* thermalization [43,44]. The starting point of bottom-up thermalization is an ensemble of too few particles particles $f \ll 1$ with too high momenta $p \gg T$ compared to thermal equilibrium with the final temperature T. In the bottom-up process, the collisions among these few hard particles lead to soft radiation that forms a soft thermal bath with a temperature $T_s \ll T$. The further interaction between the hard particles and soft thermal bath eventually causes a radiational breakup of the hard particles that heats the soft thermal bath to its final temperature T. We will consider how this picture is quantitatively changed when pushing to finite and small values of λ. We see that the NLO corrections are under quantitative control for $\lambda \lesssim 10$, and we observe that the NLO corrections make thermalization faster.

For a second system, we consider an overoccupied, $f \gg 1$ initial state in its *self-similar scaling solution*, that is, a nonthermal, time-dependent fixed point that is rapidly reached from any overoccupied initial condition—see Refs. [44–49]. In this case too, we find that NLO corrections bring about a faster thermalization and that, while a bit larger than the underoccupied scenario, they remain under control over a wide range of couplings.

II. SETUP

A. Leading-order kinetic theory

In the weak-coupling limit $\lambda \to 0$, the evolution of modes with perturbative occupancies $\lambda f(p) \ll 1$ and whose momenta are larger than the screening scale $p^2 \gg m^2$ can be described to leading order in λf by an effective kinetic equation for the color averaged gauge boson distribution function [32]

$$\partial_t f(p,t) = -\mathcal{C}_{2\leftrightarrow 2}[f](p) - \mathcal{C}_{1\leftrightarrow 2}[f](p). \tag{1}$$

The elastic $2 \leftrightarrow 2$ scattering and collinear $1 \leftrightarrow 2$ splitting parts of the collision operator—whose precise forms are given in Appendix A 1—depend, respectively, on effective matrix elements $|\mathcal{M}|^2$ and splitting rates γ, which have been discussed in detail in Refs. [19,32,49,50]. The elastic collision term includes LO screening effects by consistently regulating the Coulombic divergence in t and u channels at the scale m. The splitting kernel includes the effects of LPM suppression [34–36,51–53] which regulate collinear divergences. These effects depend on m and an effective temperature T_*,

$$m^2 = 4\lambda \int_{\mathbf{p}} \frac{f_p}{p}, \quad T_* = \frac{2\lambda}{m^2} \int_{\mathbf{p}} f_p(1+f_p), \tag{2}$$

which are self-consistently calculated during the simulation. The effective theory contains no free parameters besides the coupling constant λ. Our numerical implementation is the discrete-p method of Ref. [49].

B. Next-to-leading-order kinetic theory

NLO corrections to this kinetic picture are derived in Ref. [54] for a dilute set of high-energy "jet" partons interacting with a thermal medium and in Ref. [41] at first order in the departure from equilibrium, suited for the determination of transport coefficients. These $\mathcal{O}(\sqrt{\lambda})$ corrections arise from the self-interactions of soft gluons with $p \sim m \sim \sqrt{\lambda}T$ appearing in the internal lines in the diagrammatic computation of the collision kernels. At this order, these soft gluons can be treated as classical fields, retaining only the T/p-enhanced part of their equilibrium distribution, and their contributions can be treated within the hard thermal loop (HTL) effective theory [33]. Furthermore, they can be treated analytically without recurring to brute-force HTL computations, owing to the light-cone techniques introduced in Refs. [38,54,55] (see Ref. [56] for a more pedagogical exposition).

These calculations can be extended also to some far-from-equilibrium systems. As it is known (see, e.g., Refs. [19,41,57–59]), for $p \ll T_*$, the collinear splittings are very effective and rapidly build up a *soft thermal tail*. That is, they ensure that $f(m \lesssim p \ll T_*) \approx T_*/p$. This, in turn, implies that, in cases with isotropic initial conditions, the collision operator can naturally accommodate the NLO corrections derived in Refs. [41,54]. The NLO corrections are suppressed—with respect to the LO terms in Eq. (1)—by a factor of $\lambda T_*/m$. This arises from the product of the naive suppression factor for loops λ with the occupation

number at the scale $p \sim m$, that is $\lambda f(m) \approx \lambda T_*/m$.[1] Isotropy further ensures that the terms which have not been determined in the "almost NLO" determination of Ref. [41] do not contribute here, guaranteeing that what we are presenting is the full set of NLO modifications.

These $\mathcal{O}(\lambda T_*/m)$ contributions, which we discuss in more detail in Appendix A 2, consist of new scattering processes and modifications to the LO ones, as shown in Refs. [41,54]. The rate of soft $2 \leftrightarrow 2$ scattering is modified. This modification, and an $\mathcal{O}(\lambda T_*/m)$ correction to the in-medium dispersion, also provide an $\mathcal{O}(\lambda T_*/m)$ shift in the $1 \leftrightarrow 2$ rate. This $1 \leftrightarrow 2$ splitting rate must furthermore be corrected wherever one participant becomes soft or when the opening angle becomes less collinear.

A rather general property of kinetic theory resummations is that it is possible to construct collision operators that are equivalent up to a given order but differ by subleading corrections. This was exploited in Refs. [19,49] to construct a LO implementation that is numerically well behaved, thanks to a partial resummation of higher-order effects; a subtraction will thus be needed to ensure that no double-counting takes place.

We exploit this same property at NLO: as we shall show in detail in Appendix A 2, we construct two separate collision operators, both including all $\mathcal{O}(\lambda T_*/m)$ effects but differing at higher orders. We call these two schemes scheme 1 and scheme 2. The difference in the results obtained from these two, as well as their spread from the LO results, can be taken as an estimate of the uncertainty, in particular when extrapolating toward regions where the expansion parameters are no longer small. One such region is thus $\lambda T_*/m \gtrsim 1$, while another arises in the region where $p \gg T_*$. As is known (see the detailed discussion in Ref. [50]), the *formation time* for a collinear splitting process grows with p/T_*, making the splitting process sensitive not just to the frequent soft scatterings exchanging $q \sim m$, but also to the rarer higher-momentum exchanges. For $p/T_* \gtrsim T_*^2/(\lambda m^2)$, our form of the LO and NLO $1 \leftrightarrow 2$ rate, which only includes $q \sim m$ scatterings, becomes inaccurate. As we elaborate in Appendix A 2, our first implementation, scheme 1, treats these processes with no partial resummation of higher-order effects, and the collision kernel is more prone to extrapolate to (unphysical) negative values than our second, nonstrict implementation, scheme 2.

C. Initial conditions

For the underoccupied initial condition, we will use a Gaussian form centered around a characteristic momentum scale Q, as in Ref. [19]. To mimic the situation in the last stage of bottom-up thermalization (and for numerical stability), we embed this distribution of hard particles in a soft thermal bath that carries 10% of the total energy density

$$f(p) = Ae^{-\frac{(p-Q)^2}{(Q/10)^2}} + n_B(p, T_{\text{init}}), \tag{3}$$

where A and T_{init} are $A \approx (0.419Q/T)^{-4}$ and $T_{\text{init}}/T \approx 0.562$. n_B is the equilibrium Bose-Einstein distribution.

In the overoccupied case, we let the system evolve from the scaling solution [49]

$$\tilde{f}(\tilde{p}) = (0.22e^{-13.3\tilde{p}} + 2.0e^{-0.92\tilde{p}^2})/\tilde{p}, \tag{4}$$

where $\tilde{p} \equiv (p/Q)(Qt)^{-1/7}$ and $f(p) \equiv (Qt)^{-4/7}\lambda^{-1}\tilde{f}(\tilde{p})$. For this initial condition, one has $\langle p \rangle \ll T$, and a direct energy cascade from the IR to the UV takes place. We choose Q and an initial time t_0 such that $f \gg 1$.

III. RESULTS

The thermalization processes of systems initialized with Eqs. (3) and (4) are displayed in Fig. 1 for $Q = 50$ and $\lambda = 5$ for the underoccupied case (left panel) and $\lambda = 1$ for the overoccupied case (right panel). Both are evolved with the scheme 2 prescription.

The NLO evolutions of these systems exhibit the same qualitative features as their LO counterparts. In the case of underoccupied initial conditions, the NLO evolution shows the characteristic features of bottom-up thermalization: one can see the hard particles lose energy through the radiational cascade heating the soft thermal bath. Eventually, the system thermalizes as the hard particles are quenched in the thermal bath [44]. In the case of the overoccupied initial conditions, the direct energy cascade to the UV seen at LO is also seen at NLO. The departure from the scaling solution takes place once $\langle p \rangle \sim T$, corresponding to $f(p) \sim 1$.

To determine thermalization times of these systems, we characterize them in terms of effective temperatures T_α,

$$T_\alpha = \left[\frac{2\pi^2}{\Gamma(\alpha+3)\zeta(\alpha+3)} \int \frac{d^3p}{(2\pi)^3} p^\alpha f(p)\right]^{\frac{1}{\alpha+3}},$$

which all coincide with T in equilibrium but differ for nonequilibrium systems. We then define a (kinetic) thermalization time by demanding that the different effective temperatures are sufficiently close to each other. Specifically, we define the (kinetic) thermalization time using the condition [21]

$$(T_0(t_{\text{eq}})/T_1(t_{\text{eq}}))^{\pm 4} = 0.9, \tag{5}$$

where we use "+" and "−" for under- and overoccupied systems, respectively. For the underoccupied (overoccupied) system in Fig. 1, this condition is fulfilled for $\lambda^2 Tt \approx 1029$ ($\lambda^2 Tt \approx 67$), denoted by the green dashed

[1] In equilibrium, $\lambda T_*/m \sim g$ becomes the well-known suppression factor g of loops at the screening scale gT.

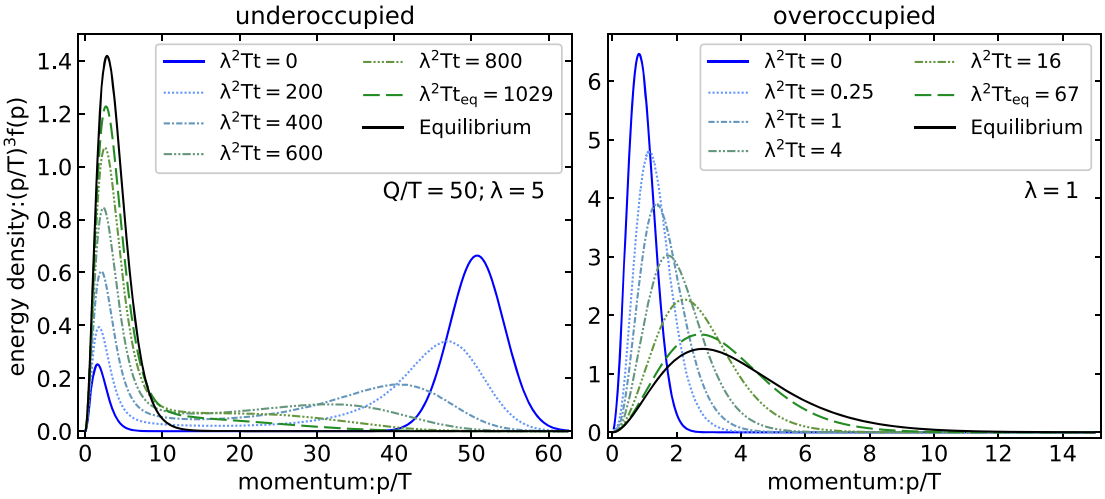

FIG. 1. Time evolution from the initial conditions (3)–(4) in solid blue lines to the final equilibrium state in solid black. The dotted and dashed lines show intermediate steps upon solving the NLO kinetic theory (scheme 2). The values of the couplings are $\lambda = 5$ and $\lambda = 1$, respectively.

line. At this point, most of the energy is in the thermal bath, rather than in the initial UV (IR) structure.

We have determined this thermalization time for different values of the coupling constant λ and, in the underoccupied case, a variety of initial momenta Q, using both the LO as well as the two NLO schemes; the under- and overoccupied-case results are documented in Tables I and II and displayed in Fig. 2. Our main findings are as follows:

(i) The qualitative effect of the NLO corrections is to reduce the time required for thermalization.

(ii) NLO corrections are well under control for a wide range of coupling constants.

In the regime of small values of $\lambda \lesssim 3$—corresponding to $m \lesssim T$ in equilibrium, so that the scale separations assumed in the derivation of the kinetic theory are fulfilled—the NLO corrections constitute merely a 5% and 20% reduction of the thermalization time in the under- and overoccupied cases. It is reassuring to observe that, in both scenarios, results from the two NLO schemes are close to each other compared to the overall size of the NLO correction. In the

TABLE I. Table of thermalization times $\hat{t}_{\rm eq} \equiv \lambda^2 T t_{\rm eq}$ of underoccupied initial conditions with different Q/T and values of the coupling λ.

Q/T	λ	$\hat{t}_{\rm eq}^{\rm LO}$	$\hat{t}_{\rm eq}^{\rm NLO1}$	$\hat{t}_{\rm eq}^{\rm NLO2}$	Q/T	λ	$\hat{t}_{\rm eq}^{\rm LO}$	$\hat{t}_{\rm eq}^{\rm NLO1}$	$\hat{t}_{\rm eq}^{\rm NLO2}$
20	1	503.4	465.2	473.2	35	0.1	623.4	614.5	615.7
40	1	818.7	784.1	791.8	35	0.5	707.5	683.3	687.6
60	1	1060.0	1039.1	1044.4	35	1	749.3	712.5	720.7
80	1	1263.9	1261.5	1263.2	35	5	859.4	764.5	803.4
100	1	1443.4	1462.2	1459.8	35	10	910.5	774.3	849.5
20	5	588.4	489.5	528.8	50	0.1	798.9	791.7	793.3
40	5	934.6	845.5	882.4	50	0.5	897.3	878.6	882.0
60	5	1193.8	1142.4	1163.5	50	1	945.5	916.9	923.6
80	5	1409.5	1410.4	1408.9	50	5	1070.9	998.6	1028.7
100	5	1599.2	1661.6	1630.4	50	10	1129.1	1027.6	1086.4

TABLE II. Table of thermalization times $\hat{t}_{\rm eq} \equiv \lambda^2 T t_{\rm eq}$ of overoccupied initial conditions with different values of the coupling λ.

λ	0.01	0.03	0.06	0.1	0.3	0.6	1	3	6	10
$\hat{t}_{\rm eq}^{\rm LO}$	40.9	46.2	50.4	54.0	63.2	70.4	76.2	89.5	97.1	101.0
$\hat{t}_{\rm eq}^{\rm NLO1}$	40.5	45.4	49.1	52.0	58.8	62.9	65.4	67.1	64.1	59.3
$\hat{t}_{\rm eq}^{\rm NLO2}$	40.5	45.4	49.1	52.1	59.1	63.6	66.6	71.1	71.7	70.7

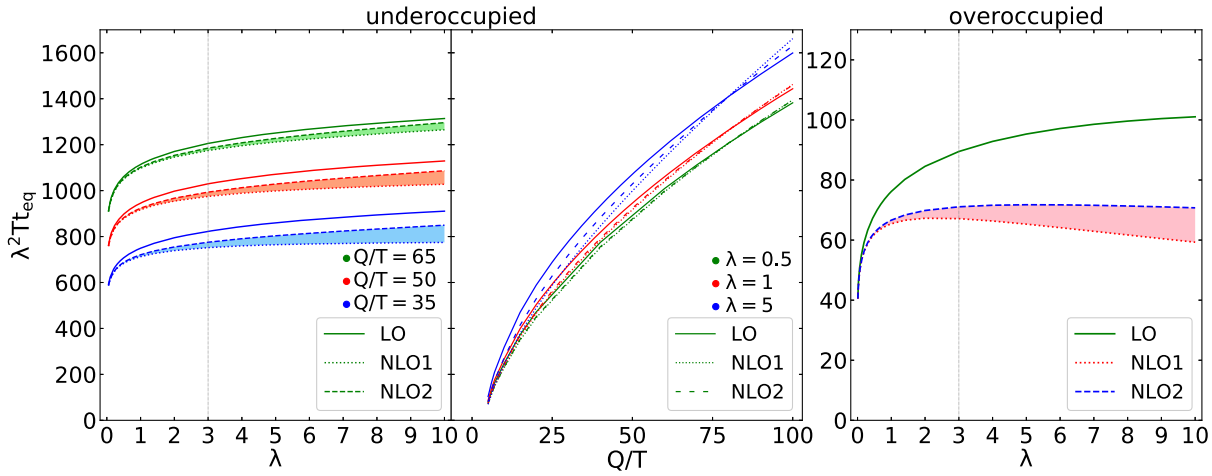

FIG. 2. Equilibration times as a function of the coupling and, in the underoccupied case, the initial UV scale. The shaded band between the two NLO schemes can be taken as a first indication of the theory uncertainty. The coupling $\lambda = 3$ for which $m = T$ in thermal equilibrium is indicated by a vertical gray line.

$\lambda \to 0$-limit, the difference between the two NLO schemes vanishes faster than their difference to LO. This demonstrates that the observed differences from the LO are true NLO corrections and are not contaminated by the scheme differences that affect the result beyond the NLO accuracy.

Extrapolating to higher values of $3 \lesssim \lambda \lesssim 10$, we see that in the underoccupied case the difference between the two NLO schemes becomes comparable to the size of the of the NLO correction itself. This indicates quantitative sensitivity to corrections beyond NLO. However, taking the difference of the two schemes as an estimate of the uncertainty, we observe that, strikingly, the corrections remain below 10% level even for these large value of the coupling. In the overoccupied case, the correction reaches 40% level, with only a moderate spread between the two schemes.

At leading order, the underoccupied thermalization time is parametrically (up to logarithms) of order $t_{\rm eq} \sim (\lambda^2 T)^{-1}(Q/T)^{1/2}$ [44], related to the democratic splitting time of the particles at the scale Q in a thermal bath with temperature T. At NLO, corrections are expected to arise at the relative order $\lambda T/m \sim \sqrt{\lambda}$. We find that that LO thermalization time given in Eq. (5) is well described for $\lambda < 5$ by a fit,[2]

$$\lambda^2 T t_{\rm eq}^{\rm LO} \approx (Q/T)^{1/2}(173. + 9.8\log\lambda) - 277. \qquad (6)$$

For small $\lambda < 1$ and $20 < Q < 80$, the NLO correction in both schemes is approximately given by

$$\frac{t_{\rm eq}^{\rm LO}}{t_{\rm eq}^{\rm NLO}} \approx 1 + \lambda^{1/2}\left(0.22 - 0.05\log\left(\frac{Q}{T}\right)\right), \qquad (7)$$

and similarly for the overoccupied case,

$$\lambda^2 T t_{\rm eq}^{\rm LO} \approx \frac{76.}{1 - 0.19\log\lambda}, \quad \frac{t_{\rm eq}^{\rm LO}}{t_{\rm eq}^{\rm NLO}} \approx 1 + 0.14\lambda^{1/2}. \qquad (8)$$

IV. CONCLUSIONS

The poor convergence of the perturbative series for several different quantities has limited its usefulness in many phenomenological applications. The soft corrections studied here are responsible for this poor convergence for many observables such as transport coefficients [41,42] or momentum broadening coefficients [37,38]. For these quantities, NLO corrections completely overtake the LO results for $\lambda \approx 10$. On the contrary, in the present case of isotropic thermalization, these soft corrections seem to be well under control; the corrections are at most of order 40% for the overoccupied case at $\lambda \approx 10$. These findings are ostensibly in sharp contrast.

However, it is important to note that Ref. [41] found NLO corrections to transport coefficients to be numerically dominated by the NLO contribution to the isotropization rate governed by the transverse momentum broadening coefficient $\hat{q}$ (which obtains a large positive NLO correction [38]). The key difference with respect to the present case is that, in an *isotropic* setting, the dependence on $\hat{q}$ is significantly reduced. Instead of explicitly entering the calculation as an isotropization rate, $\hat{q}$ only appears in our case as the source of $1 \leftrightarrow 2$ splittings; it does make their rate larger, but its numerical effect is moderated by the fact that, parametrically, the LPM-suppressed $1 \leftrightarrow 2$ splitting rate is $\propto \sqrt{\hat{q}}$, whereas isotropization is $\propto \hat{q}$. Furthermore, the other NLO corrections to splitting arising from a soft

[2]Note that this thermalization time approximately agrees with that of Ref. [19] but differs slightly due to slightly different initial conditions and the precise definition of thermalization time used here.

participant, a wider-angle emission, or a rarer larger-momentum radiation-inducing scattering tend to decrease the rate, partially canceling the $\sqrt{\hat{q}}$-driven increase. This partial cancellation was already seen in the thermal photon production rate—another isotropic observable—which also shows moderate NLO corrections [40]. This is suggestive of a pattern which we think deserves further investigations. We note that some of these issues may be ameliorated in thermal equilibrium by nonperturbative determination of the soft contributions developed in Refs. [60–64]. However, it is currently not known how these methods could be extended to far-from-equilibrium systems.

Lastly, we point out that, when trying to apply our methods to anisotropic systems, such as one undergoing Bjorken (one-dimensional) expansion, we would necessarily need to include the isotropizing effect of transverse momentum broadening, further compounded by the emergence of plasma instabilities [44,65–69]. However, in the final stages of the bottom-up thermalization of heavy-ion collisions, the hard particles interact mainly with the isotropic soft thermal bath. This suggests that the methods developed here may be extended to improve the phenomenological description of the bottom-up hydrodynamization in heavy-ion collision.

ACKNOWLEDGMENTS

J. G. acknowledges support by a PULSAR grant from the Région Pays de la Loire. S. I. and Y. F. were supported in part by the National Natural Science Foundation of China under Grants No. 11935007, No. 11221504, No. 11890714, and No. 11861131009. We are grateful to Peter Arnold for useful conversations.

APPENDIX: DEFINITIONS AND IMPLEMENTATIONS OF THE KINETIC THEORY

1. Leading-order kinetic theory

The precise form of the LO collision operator reads[3]

$$\mathcal{C}_{2\leftrightarrow 2}[f](p) = \int_{\mathbf{k},\mathbf{p}',\mathbf{k}'} \frac{|\mathcal{M}(m)|^2 (2\pi)^4 \delta^{(4)}(p+k-p'-k')}{22k2k'2p2p'} \times \{f_p f_k [1+f_{p'}][1+f_{k'}] - f_{p'} f_{k'} [1+f_p] \times [1+f_k]\}, \tag{A1}$$

$$\mathcal{C}_{1\leftrightarrow 2}[f](p) = \frac{(2\pi)^3}{2p^2}\int_0^\infty dp'dk'\gamma^p_{p',k'}(m,T_*) \times \{f_p[1+f_{p'}] \times [1+f_{k'}] - f_{p'}f_{k'}[1+f_p]\}\delta(p-p'-k') + \frac{(2\pi)^3}{p^2}\int_0^\infty dp'dk\gamma^{p'}_{p,k}(m,T_*)\delta(p+k-p') \times \{f_p f_k[1+f_{p'}] - f_{p'}[1+f_p][1+f_k]\}. \tag{A2}$$

The elastic kernel given in Eq. (A1) depends on the effective in-medium matrix element $|\mathcal{M}(m)|^2$. As the vacuum elastic scattering has a $1/t^2 \sim \frac{1}{q^4}$ (and $1/u^2$) infrared divergence, with momentum transfer $q = |\mathbf{p}-\mathbf{p}'|$, it makes the soft small angle scattering contribution to the scattering kernel diverge. This divergence is, however, regulated by the physics of in-medium screening. A prescription that is accurate to leading order is given in Ref. [49] by the replacement

$$\frac{(s-u)}{t} \to \frac{(s-u)}{t}\frac{q^2}{q^2+\xi^2 m^2}, \quad \xi_{\rm LO} = \frac{e^{5/6}}{2\sqrt{2}}, \tag{A3}$$

where at LO ξ is fixed to $\xi_{\rm LO}$, so as to reproduce the LO longitudinal momentum diffusion coefficient [54,56].

The effective medium-induced collinear splitting/merging matrix element γ is given by [32,70]

$$\gamma^p_{p',k'}(m,T_*) = \frac{\lambda}{32\pi^4 p}\frac{1+x^4+(1-x)^4}{x^3(1-x)^3}\mathrm{Im}(\boldsymbol{\nabla}_{\mathbf{b}}\cdot\boldsymbol{F}(\mathbf{0})), \tag{A4}$$

with the momentum fraction $x = k'/p$ and where $\boldsymbol{F}(\boldsymbol{b})$ resums an arbitrary number of soft elastic scatterings with the medium. It depends on two dimensionless variables,

$$\hat{M} \equiv 1-x+x^2, \quad \eta \equiv \frac{px(1-x)\lambda T_*}{m_g^2}, \tag{A5}$$

where $m_g^2 = m^2/2$ is the LO mass for gluons with $p \gg m$. Parametrically, η is the ratio squared of the formation time of the splitting process $\tau_{\rm form} \sim \sqrt{E/\hat{q}} \sim \sqrt{\frac{x(1-x)p}{\lambda T_* m^2}}$ and of the elastic scattering rate $\tau_{\rm el} \sim 1/\lambda T_*$. $\boldsymbol{F}(\boldsymbol{b})$ is the solution to this differential equation [32,54,70],

$$-2i\nabla_{\boldsymbol{b}}\delta^2(\boldsymbol{b}) = \frac{i}{2px(1-x)}(\hat{M}m_g^2 - \nabla^2_{\boldsymbol{b}})\boldsymbol{F}(\boldsymbol{b}) + \frac{1}{2}(C(b) + C(xb) + C((1-x)b))\boldsymbol{F}(\boldsymbol{b}), \tag{A6}$$

and $C(b)$ is the Fourier transform of the soft scattering rate,

$$C(b) = \int \frac{dq_\perp^2}{(2\pi)^2}(1-e^{i\boldsymbol{b}\cdot\boldsymbol{q}_\perp})\frac{d\Gamma(q_\perp)}{d^2q_\perp}. \tag{A7}$$

[3]Our matrix element is related to that of Ref. [32] by $|\mathcal{M}|^2 = \sum_{bcd}|\mathcal{M}^{ab}_{cd}|^2/\nu$, $f = f_a$, and $\gamma = \gamma^g_{gg}/\nu$. $\int_{\mathbf{p}} \equiv \int \frac{d^3p}{(2\pi)^3}$ and $\nu = 2d_A = 2(N_c^2-1)$ for gluons.

In an isotropic medium, it reads

$$C(b) = \frac{\lambda T_*}{2\pi}\left(K_0(bm) + \gamma_E + \log\left(\frac{bm}{2}\right)\right). \quad \text{(A8)}$$

By rescaling $\boldsymbol{b} = \tilde{\boldsymbol{b}}/m_g$ and $\boldsymbol{F} = 2px(1-x)/m_g^2\tilde{\boldsymbol{F}}$, the coefficient of the second line of Eq. (A6) becomes proportional to η. The method presented in Ref. [71] is then used for the numerical solution.

2. Next-to-leading-order kinetic theory

Let us start by discussing the corrections to Eq. (A4). As shown in Ref. [54], its form remains valid at NLO, but the LPM resummation in Eq. (A6) must include two $\mathcal{O}(\lambda T_*/m)$ corrections. The dispersion relation gets shifted to $m_{g\mathrm{NLO}}^2 = m_g^2 + \delta m_g^2$, and the soft scattering kernel is modified in $C_{\mathrm{NLO}}(b) = C(b) + \delta C(b)$. For an isotropic state with a T_*/p soft thermal tail, the equilibrium results for δm_g^2 [39] and $\delta C(b)$ [38,40] can be used with the replacement $T \to T_*$, $m_D \to m$. The former reads

$$\delta m_g^2 = -\frac{\lambda T_* m}{2\pi}. \quad \text{(A9)}$$

In our first implementation, i.e., *scheme 1*, we treat δm_g^2 and $\delta C(b)$ as perturbations to their LO counterparts. Hence, $\boldsymbol{F}$ is perturbed as $\boldsymbol{F}_{\mathrm{NLO}} = \boldsymbol{F} + \delta\boldsymbol{F}$, and the latter is computed exactly as in Appendix E of Ref. [54].[4] The resulting $\gamma_{\mathrm{NLO}} = \gamma + \delta\gamma$ can become problematic when extrapolated to large values of η and $\lambda T_*/m$. As per its definition, large values of η correspond to formation times larger than the mean free time for soft scatterings, so that rarer, harder scatterings, which are not included in the form (A8) of the scattering kernel, would have a chance to occur. As shown in Ref. [50], for $\eta \gtrsim (T_*/m)^4$, scatterings with $q_\perp \sim T_*$ would need to be included, which is far from trivial in an off-equilibrium setting. At LO, one can, however, expect, as in equilibrium, that the approximation introduced by extrapolating Eq. (A8) to $\eta \gtrsim (T_*/m)^4$ amounts to an overestimate of γ at the 10%–20% level. That happens because large values of η privilege the small-b form of $C(b)$, which at leading order is approximated by $\lambda T_* m^2 b^2 \ln(1/bm)$, with a coefficient that varies in equilibrium by 25% between $1/T \ll b \ll 1/m_D$ and $1/T \gg b$.

At NLO, this translates for large η into a strong sensitivity on $\delta C(b \ll 1/m) \approx -\lambda^2 T_*^2 b/(32\pi)$, which is the Fourier transform of the subleading, $\propto 1/q_\perp^3$, form of the collision kernel for $m \gg q_\perp \gg T_*$. Its negative coefficient, for large enough $\lambda T_*/m$ and η, makes γ_{NLO} negative. We thus propose a second implementation, *scheme 2*, so that the difference between the two can be taken as a proxy for the reliability of these extrapolations. In this second implementation, we do not treat δm_g^2 and $\delta C(b)$ as perturbations. We rather solve

$$-2i\nabla_{\boldsymbol{b}}\delta^2(\boldsymbol{b}) = \frac{i}{2px(1-x)}(\hat{M}\bar{m}_g{}^2 - \nabla_{\boldsymbol{b}}^2)\bar{\boldsymbol{F}}(\boldsymbol{b}) + \frac{1}{2}(C(xb) + C(b) + C((1-x)b))\left(1 + \frac{\delta C}{C}\right)\bar{\boldsymbol{F}}(\boldsymbol{b}), \quad \text{(A10)}$$

where we have defined the mass self-consistently as

$$\bar{m}_g \equiv \sqrt{m_g^2 + \frac{\lambda^2 T_*^2}{8\pi^2}} - \frac{\lambda T_*}{2\sqrt{2}\pi} \approx m_g\left(1 - \frac{\lambda T_*}{2\pi m} + \ldots\right), \quad \text{(A11)}$$

i.e., the positive solution to $\bar{m}_g^2 = m_g^2 - \lambda T_* \bar{m}_g/(\sqrt{2}\pi)$, so that, by resumming some higher-order terms, it stays positive at large $\lambda T_*/m$. In a similar spirit, we have implemented the collision kernel as

$$\frac{\delta C}{C} \equiv \frac{\delta C(b) + \delta C(xb) + \delta C((1-x)b)}{C(b) + C(xb) + C((1-x)b)} \quad \text{(A12)}$$

so that δC is not treated as a perturbation in this scheme. Hence, the difference between the two schemes, in particular at small to moderate values of $\lambda T_*/m$ and large values of p/T_*, is a measure of the uncertainty caused by the lack of harder scatterings in the implementation of LPM resummation.

The remaining genuine NLO corrections are:

(1) wider-angle "semicollinear" $1 \leftrightarrow 2$ processes,
(2) contributions to longitudinal momentum diffusion arising from soft legs in $1 \leftrightarrow 2$ processes and from soft loops in $2 \leftrightarrow 2$ processes.

We implement the two together, following Ref. [41]. This amounts to the addition of this extra $1 \leftrightarrow 2$ splitting rate,

$$\gamma^p_{p'k}|_{\mathrm{semi}} = \frac{\lambda}{64\pi^4 p}\frac{1 + x^4 + (1-x)^4}{x^3(1-x)^3}\int\frac{d^2h}{(2\pi)^2}\int\frac{d^2q_\perp}{(2\pi)^2} \times \delta C(q_\perp, \delta E) \times [V(1) + V(x) + V(1-x)], \quad \text{(A13)}$$

where

$$\delta E(\boldsymbol{h}) = \frac{h^2 + \hat{M}m_g^2}{2px(1-x)},$$
$$V(v) = \left(\frac{\boldsymbol{h}}{\delta E(\boldsymbol{h})} - \frac{\boldsymbol{h} + v\boldsymbol{q}_\perp}{\delta E(\boldsymbol{h} + v\boldsymbol{q}_\perp)}\right)^2,$$
$$\delta C(q_\perp, \delta E) = \frac{\lambda T_* m^2 (q_\perp^2 + \delta E^2)^{-1}}{(q_\perp^2 + \delta E^2 + m^2)} - \frac{\lambda T_* m^2 (q_\perp^2)^{-1}}{(q_\perp^2 + m^2)}. \quad \text{(A14)}$$

In a nutshell, this implementation subtracts the single-scattering term of Eq. (A4)—the second term in $\delta C(\boldsymbol{q}, \delta E)$

[4] $\boldsymbol{b}$ here corresponds to $p\mathbf{b}$ there; $\boldsymbol{F}_{\mathrm{NLO}}$ here corresponds to $p^3(\mathbf{F}_0 + \mathbf{F}_1)$ there. $\delta C(b)$ can be found in Ref. [40].

is precisely $d\Gamma(q_\perp)/d^2q_\perp$ in Eq. (A7)—and replaces it with a form that keeps track not only of the medium-induced changes in the transverse momentum of the particles undergoing splitting but also of the changes in the small light-cone component of the momentum, i.e., $p^0 - p^z$ for $p^0 \approx p^z \approx p$. Indeed, as shown in Refs. [40,41,54], for larger emission angles, these changes are no longer negligible with respect to those in transverse momentum and give rise to the form shown here. The soft gluon carries $q^0 - q^z = \delta E$ and is no longer kinematically constrained to mediating spacelike-only interactions with the medium.

Finally, as anticipated in the main text, we need to avoid double-countings. The $2 \leftrightarrow 2$ collision kernel in Eq. (A1) integrates over values of k, k', p' that can be of order m, with $q \sim m$ as well. In this region, the formulation in Eq. (A1) is no longer accurate. These slices of phase space can be shown to be an $\mathcal{O}(\lambda T_*/m)$ contribution [41,54], though obtained with an improper treatment for these soft modes. Thus, this contribution needs to be subtracted, as it is properly included in the NLO contribution to longitudinal momentum diffusion, incorporated in Eq. (A13). This subtraction is analogous to that discussed in Appendix B.3 of Ref. [41]. Here, we perform it by shifting the value of ξ to $\xi_{\rm NLO} \approx \xi_{\rm LO} + \mathcal{O}(\lambda T_*/m)$. We recall that the LO value of ξ is fixed by imposing that the expansion of Eq. (A1) with the replacement (A3) for $\omega \equiv p - p'$ and q much smaller than k and p matches the LO hard loop evaluation of that limit, which is proportional to the LO longitudinal momentum diffusion coefficient [54]. To get $\xi_{\rm NLO}$, we must now also expand for $k \sim \omega$, $q \ll p$, generating a term of relative order $\lambda T_*/m$. We then impose that $\xi_{\rm NLO}$ cancels this term, yielding

$$\frac{\lambda m^2}{4\pi p}\ln\frac{\mu}{m_g} = \frac{\lambda m^2\left(\frac{5}{6} + \ln\frac{\mu}{2\sqrt{2\xi m_g}}\right)}{4\pi p} + \frac{3\lambda^2 m T_* \xi}{(8\pi)^2 p}, \tag{A15}$$

where the lhs is what we impose, i.e., the hard loop form, with some UV cutoff μ, corresponding to the LO longitudinal momentum diffusion term, while the rhs contains the terms arising from the explicit expansion of Eq. (A1). Keeping only the first, leading term, we recover $\xi_{\rm LO}$. We solve Eq. (A15) self-consistently, finding $\xi_{\rm NLO}$ in terms of the Lambert function W as

$$\begin{aligned}\xi_{\rm NLO} &= -\frac{16 m\pi}{3\lambda T_*} W\left(-\frac{3e^{5/6}\lambda T_*}{32\sqrt{2}m\pi}\right) \\ &\approx \xi_{\rm LO} + \frac{3e^{5/3}T_*\lambda}{128\pi m} + \mathcal{O}\left(\frac{\lambda^2 T_*^2}{m^2}\right).\end{aligned} \tag{A16}$$

[1] J. H. Traschen and R. H. Brandenberger, Phys. Rev. D **42**, 2491 (1990).
[2] L. Kofman, A. D. Linde, and A. A. Starobinsky, Phys. Rev. Lett. **73**, 3195 (1994).
[3] L. Kofman, Lect. Notes Phys. **738**, 55 (2008).
[4] M. Drees and B. Najjari, J. Cosmol. Astropart. Phys. 10 (2021) 009.
[5] A. D. Linde, Rep. Prog. Phys. **42**, 389 (1979).
[6] A. Mazumdar and G. White, Rep. Prog. Phys. **82**, 076901 (2019).
[7] A. D. Sakharov, Pis'ma Zh. Eksp. Teor. Fiz. **5**, 32 (1967).
[8] P. Di Bari, Prog. Part. Nucl. Phys. **122**, 103913 (2022).
[9] D. G. Figueroa, A. Florio, F. Torrenti, and W. Valkenburg, J. Cosmol. Astropart. Phys. 04 (2021) 035.
[10] D. G. Figueroa, A. Florio, F. Torrenti, and W. Valkenburg, arXiv:2102.01031.
[11] Z. Citron *et al.*, CERN Yellow Rep. Monogr. **7**, 1159 (2019).
[12] D. Banerjee, M. Bögli, M. Dalmonte, E. Rico, P. Stebler, U. J. Wiese, and P. Zoller, Phys. Rev. Lett. **110**, 125303 (2013).
[13] J. Berges, K. Boguslavski, S. Schlichting, and R. Venugopalan, Phys. Rev. Lett. **114**, 061601 (2015).
[14] D. Paulson, L. Dellantonio, J. F. Haase, A. Celi, A. Kan, A. Jena, C. Kokail, R. van Bijnen, K. Jansen, P. Zoller, and C. A. Muschik, PRX Quantum **2**, 030334 (2021).
[15] J. Berges, M. P. Heller, A. Mazeliauskas, and R. Venugopalan, Rev. Mod. Phys. **93**, 035003 (2021).
[16] S. Schlichting and D. Teaney, Annu. Rev. Nucl. Part. Sci. **69**, 447 (2019).
[17] S. Grozdanov and W. van der Schee, Phys. Rev. Lett. **119**, 011601 (2017).
[18] A. Folkestad, S. Grozdanov, K. Rajagopal, and W. van der Schee, J. High Energy Phys. 12 (2019) 093.
[19] A. Kurkela and E. Lu, Phys. Rev. Lett. **113**, 182301 (2014).
[20] A. Kurkela and A. Mazeliauskas, Phys. Rev. Lett. **122**, 142301 (2019).
[21] A. Kurkela and A. Mazeliauskas, Phys. Rev. D **99**, 054018 (2019).
[22] X. Du and S. Schlichting, Phys. Rev. D **104**, 054011 (2021).
[23] X. Du and S. Schlichting, Phys. Rev. Lett. **127**, 122301 (2021).
[24] A. Kurkela, A. Mazeliauskas, J.-F. Paquet, S. Schlichting, and D. Teaney, Phys. Rev. Lett. **122**, 122302 (2019).
[25] A. Kurkela, A. Mazeliauskas, J.-F. Paquet, S. Schlichting, and D. Teaney, Phys. Rev. C **99**, 034910 (2019).
[26] A. Kurkela, A. Mazeliauskas, and R. Törnkvist, J. High Energy Phys. 11 (2021) 216.
[27] S. Davidson and S. Sarkar, J. High Energy Phys. 11 (2000) 012.
[28] K. Harigaya and K. Mukaida, J. High Energy Phys. 05 (2014) 006.

[29] K. Mukaida and M. Yamada, J. Cosmol. Astropart. Phys. 02 (2016) 003.
[30] S. Jeon, Phys. Rev. D **52**, 3591 (1995).
[31] S. Jeon and L. G. Yaffe, Phys. Rev. D **53**, 5799 (1996).
[32] P. B. Arnold, G. D. Moore, and L. G. Yaffe, J. High Energy Phys. 01 (2003) 030.
[33] E. Braaten and R. D. Pisarski, Nucl. Phys. **B337**, 569 (1990).
[34] L. D. Landau and I. Pomeranchuk, Dokl. Akad. Nauk Ser. Fiz. **92**, 735 (1953).
[35] L. D. Landau and I. Pomeranchuk, Dokl. Akad. Nauk Ser. Fiz. **92**, 535 (1953).
[36] A. B. Migdal, Dokl. Akad. Nauk Ser. Fiz. **105**, 77 (1955).
[37] S. Caron-Huot and G. D. Moore, Phys. Rev. Lett. **100**, 052301 (2008).
[38] S. Caron-Huot, Phys. Rev. D **79**, 065039 (2009).
[39] S. Caron-Huot, Phys. Rev. D **79**, 125002 (2009).
[40] J. Ghiglieri, J. Hong, A. Kurkela, E. Lu, G. D. Moore, and D. Teaney, J. High Energy Phys. 05 (2013) 010.
[41] J. Ghiglieri, G. D. Moore, and D. Teaney, J. High Energy Phys. 03 (2018) 179.
[42] J. Ghiglieri, G. D. Moore, and D. Teaney, Phys. Rev. Lett. **121**, 052302 (2018).
[43] R. Baier, A. H. Mueller, D. Schiff, and D. T. Son, Phys. Lett. B **502**, 51 (2001).
[44] A. Kurkela and G. D. Moore, J. High Energy Phys. 12 (2011) 044.
[45] J. Berges, S. Scheffler, and D. Sexty, Phys. Lett. B **681**, 362 (2009).
[46] J. Berges, S. Schlichting, and D. Sexty, Phys. Rev. D **86**, 074006 (2012).
[47] S. Schlichting, Phys. Rev. D **86**, 065008 (2012).
[48] A. Kurkela and G. D. Moore, Phys. Rev. D **86**, 056008 (2012).
[49] M. C. Abraao York, A. Kurkela, E. Lu, and G. D. Moore, Phys. Rev. D **89**, 074036 (2014).
[50] P. B. Arnold and C. Dogan, Phys. Rev. D **78**, 065008 (2008).
[51] A. B. Migdal, Phys. Rev. **103**, 1811 (1956).
[52] R. Baier, Y. L. Dokshitzer, A. H. Mueller, S. Peigne, and D. Schiff, Nucl. Phys. **B483**, 291 (1997).
[53] B. Zakharov, JETP Lett. **63**, 952 (1996).
[54] J. Ghiglieri, G. D. Moore, and D. Teaney, J. High Energy Phys. 03 (2016) 095.
[55] P. Aurenche, F. Gelis, and H. Zaraket, J. High Energy Phys. 05 (2002) 043.
[56] J. Ghiglieri and D. Teaney, Int. J. Mod. Phys. E **24**, 1530013 (2015).
[57] J. Hong and D. Teaney, Phys. Rev. C **82**, 044908 (2010).
[58] M. C. Abraao York, A. Kurkela, E. Lu, and G. D. Moore, Phys. Rev. D **89**, 074036 (2014).
[59] J.-P. Blaizot, J. Liao, and Y. Mehtar-Tani, Nucl. Phys. **A961**, 37 (2017).
[60] M. Panero, K. Rummukainen, and A. Schäfer, Phys. Rev. Lett. **112**, 162001 (2014).
[61] G. D. Moore and N. Schlusser, Phys. Rev. D **101**, 014505 (2020); **101**, 059903(E) (2020).
[62] G. D. Moore and N. Schlusser, Phys. Rev. D **102**, 094512 (2020).
[63] G. D. Moore, S. Schlichting, N. Schlusser, and I. Soudi, J. High Energy Phys. 10 (2021) 059.
[64] M. Laine, Eur. Phys. J. C **72**, 2233 (2012).
[65] S. Mrowczynski, Phys. Lett. B **214**, 587 (1988); **656**, 273(E) (2007).
[66] S. Mrowczynski and M. H. Thoma, Phys. Rev. D **62**, 036011 (2000).
[67] A. Kurkela and G. D. Moore, J. High Energy Phys. 11 (2011) 120.
[68] S. Hauksson, S. Jeon, and C. Gale, Phys. Rev. C **103**, 064904 (2021).
[69] S. Hauksson, S. Jeon, and C. Gale, Phys. Rev. C **105**, 014914 (2022).
[70] P. B. Arnold, G. D. Moore, and L. G. Yaffe, J. High Energy Phys. 06 (2002) 030.
[71] J. Ghiglieri and G. D. Moore, J. High Energy Phys. 12 (2014) 029.